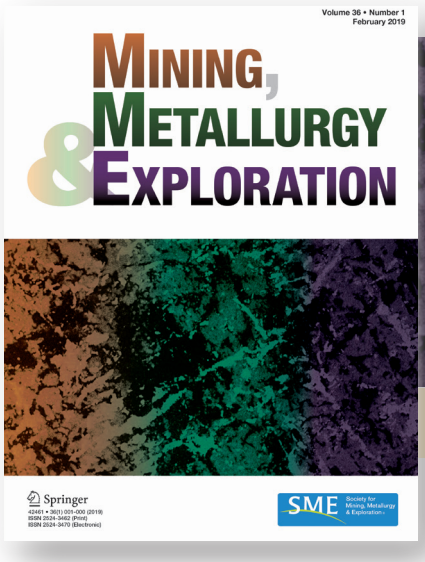

Mining, Metallurgy & Exploration

An Official International Peer-reviewed Journal of the Society for Mining, Metallurgy & Exploration

MME papers now available on Clarivate's Web of Science

Look out for the *Mining, Metallurgy & Exploration* (**MME**) journal's papers in Clarivate's Web of Science, where **MME** papers are indexed in Science Citation Index Expanded and Current Contents/Engineering, Computing & Technology.

As an SME member, you can read and download for free all of the full-text papers in the journal, including all of the archived papers of *Minerals & Metallurgical Processing* (**MMP**) as well as Online First articles, which are accepted articles that are published online first before going into issues.

MME is a continuation of **MMP**, the journal that SME has been publishing since 1984, with the scope widened to provide a balanced insight into the fields of mining, mineral/metallurgical processing and geology, and an avenue for cross-linkings among these fields. It is published in partnership with Springer Nature, one of the world's leading global research, educational and professional publishers.

In the following section, we feature six special extended abstracts of the papers published in **MME**. They are summaries of the papers distilled into about 1,000 words, starting with a description of the key takeaway of the paper: Why is it important? How can it be used if applied in real life?

You can skim through them in minutes, then stop and browse those that interest you, and as an SME member, you can read the full text of any or all of the papers for free and even download free PDFs for your personal use. And when it's time to tell others about your own work, what better avenue is there than **MME**?

To give feedback, email Chee Theng at theng@smenet.org. ■

SME MEMBERS, you can read and download full-text PDFs of all of MME and MMP* papers for free:

- **Go to www.smenet.org/login. Sign in with your email address and password.**
- **Hover your mouse over "Publications and Resources" in the top banner. Click on "Mining, Metallurgy & Exploration (MME) Journal" in the pull-down menu.**
- **Scroll down and click on the "Read the MME Journal Online" button.**

(For papers that are already in issues, click Browse Volumes & Issues in the blue banner.)

It's that SIMPLE!

NONMEMBERS, you can go to www.springer.com/engineering/journal/42461 for paid access or join SME for free access! Sign up to join at www.smenet.org/join

***MME now includes all of the archives of the *Minerals & Metallurgical Processing* journal for free access and download.**

Know what's happening in your field

Discover what's happening in other fields

Submit a paper on your work for your peers to read

Skim

Browse

Download

MME Extended Abstracts

Mining, Metallurgy & Exploration

ISSN: 2524-3462 (print version)
ISSN: 2524-3470 (electronic version)
Springer Journal No. 42461
2018 Impact Factor 0.784

• springer.com/42461
• www.smenet.org/publications-resources/publications/mining,-metallurgy-exploration-(mme)

Published since 1984 by the Society for Mining, Metallurgy & Exploration (SME).
Published with Springer from 2019 (Vol. 36).
Six issues a year (even months)

Subscriptions:
To subscribe, send an email to **journals-ny@springer.com**

SME Member
Electronic only: Automatically FREE with membership (join at www.smenet.org/join); Print and electronic: $129

Nonmember
Electronic only: $139; Print and electronic: $159

AIST/SPE/TMS member
Electronic only: $109; Print and electronic: $129

Libraries and Institutions
Print and electronic: $629

Contents

For "Aims and Scope" and to submit your paper, go to springer.com/42461

Energy dissipation and fragmentation of granite core during high-velocity impact

Jeffrey C. Johnson[1], Sindhoora Puvvada[2], Ying Lu[2], Chen-Luh Lin[2] and Jan D. Miller[2,*]
[1]Department of Mining Engineering, University of Utah, Salt Lake City, UT, USA
[2]Department of Metallurgical Engineering, University of Utah, Salt Lake City, UT, USA
[*]Corresponding author email: jan.miller@utah.edu

Full-text paper:
Mining, Metallurgy & Exploration (2019) 36:839–849, https://doi.org/10.1007/s42461-019-0068-4

Keywords: Fragmentation, Energy dissipation, Particle size, Particle shape, Bond work index, Hustrulid bar test, Zone of damage, X-ray tomography

To read the full text of this paper (free for SME members), see the beginning of this section for step-by-step instructions.

Special Extended Abstract

The amount of energy used to break rock is of interest in mine-to-mill operations to minimize energy consumption during blasting at the mine site and comminution at the processing plant. In this research, a direct energy measurement was made using high-velocity impact to cause breakage of long granite cores, and to study the energy dissipation along the entire bar length. The results show the formation of three zones of damage — fragmentation, fracture and elastic — that have been characterized in 3D using X-ray tomography. The fragmentation zone of the granite bars was studied in detail to describe the particle size distribution and the particle shape characteristics. The experimental energy dissipation in the fragmentation zone was found to be in close agreement with the expected energy calculated from the Bond work index (BWI) equation [1] when the anisotropic granite particles in the fragmentation zone are defined by length rather than by sieve size. The results increase our understanding of rock breakage and energy consumption and may find future applications in mine-to-mill operations.

Methods and procedures

The test methods and procedures performed on granite bars and their remains from high-velocity impact experiments include the measurement of the applied initial energy and the decay of energy along a bar followed by examination of the bar remains using X-ray tomography imaging and 3D analysis of the tomographic images, along with particle separation.

Energy measurement results

The granite bars were tested using a modification of the split Hopkinson pressure bar (SHPB) apparatus called the Hustrulid bar (HB) [2]. The experiment consists of a gas gun that fires a small steel striker bar on a much longer steel bar called the incident bar that is placed in direct contact with a granite bar. The steel striker and incident bars are required for elastic behavior and in the equations used for energy calculation.

The striker bar energy, calculated by the kinetic energy

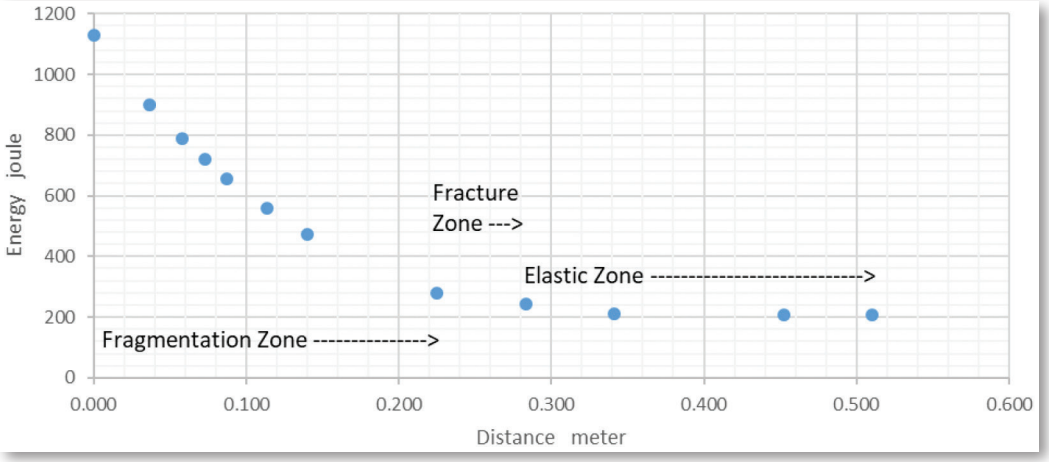

Fig. 1 Calculated energy versus distance at measurement locations along the length of the granite bar.

equation, was 2,629 J. Because the striker and incident bars are both made of steel, mechanical impedance is minimized, and most (82.5 percent) of the kinetic energy from the striker bar is transferred as strain energy into the incident bar of 2,168 J.

When the energy in the incident bar contacts the granite bar, some of it is reflected by mechanical impedance and some enters the granite bar, until damage to the granite bar severs contact with the incident bar and the remainder of the input energy is reflected. The total reflected energy was 1,040 J. The difference between the applied and reflected energy equals the initial energy applied to the granite bar: 2,168 – 1,040 J = 1,128 J.

The energy entering the granite bar decays exponentially as it is consumed in damage. The greatest decay of energy occurs in the fragmentation zone 1. The least decay of energy occurs in the elastic zone 3, where there is no damage. Between zones 1 and 3 is a transition damage zone 2, where the granite is fractured. All three zones have unique decay constants and exponents that depend on rock type.

Over the fragmentation zone length of 0.225 m, the initial energy drops from 1,128 J to 280 J (Fig. 1). The absorption of energy in the fragmentation zone is the difference between the applied energy and the energy remaining after it passed through the fragmentation zone: 1,128 – 280 = 848 J.

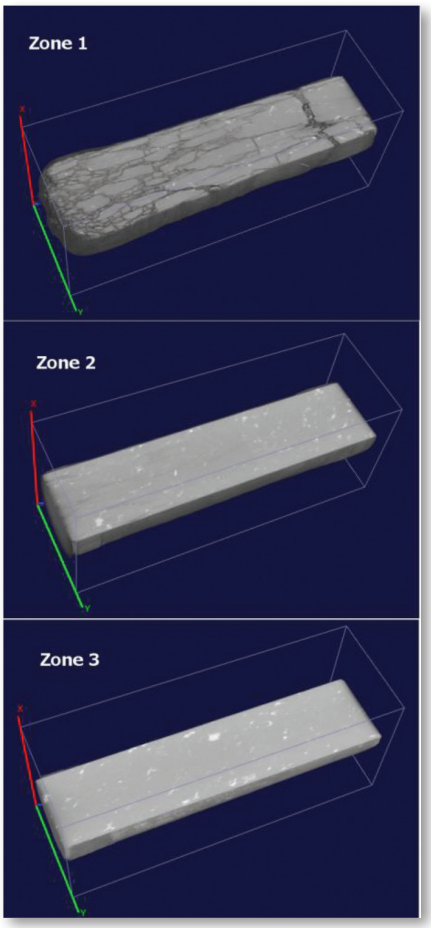

Fig. 2 Sectional views of volume rendered images from fragmented zone 1, fracture zone 2, and elastic zone 3, from granite bar test after removing half of its volume.

X-ray computed tomography (XCT) results

To better understand the fracturing process, a granite bar was covered in plastic wrap before testing. While the majority of the fragmentation zone was severed from the bar, some of its fragmented remains were held together in place by the plastic wrap. Because of the XCT machine specimen size limitations, the remains of the granite bar were cut into three 25-cm (10-inch)-long sections. These three sections — fragmentation zone 1, fractured zone 2 and elastic zone 3 — were shipped to be imaged by X-ray computed tomography (XCT) using the Carl Zeiss VoluMax 800 scanner. Figure 2 shows the volume rendered images from the three cut zones of the granite bar — zones 1, 2 and 3 — with half of each zone volume removed.

The internal image from Fig. 2 zone 1 shows some of the bar remains near the end of the fragmentation zone (left) as it transitions to the fracture zone (right). The fragmentation in zone 1 has well-defined particles in the first 25 cm. Fragmentation transitions to linear structures containing smaller fragments interspersed among larger fragments. The anisotropic particle shape is a feature associated with the unidirectional compression wave. Zone 2 is characterized by longitudinal cracks propagating in the direction of the compression wave that extend an additional 25 cm. In the elastic zone 3, cracking is not evident at the voxel resolution of 125 μm, and the core appears to be without damage. As expected, the extent of damage decreases along the length of the core from impact.

Because of the anisotropic shape, particles from the fragmentation zone were sized by length as the characteristic dimension, and the results are presented in Table 1, which reveal an 80 percent passing size of 60 mm.

Comparison of measured energy to that calculated from the BWI equation

The energy consumed in the fragmentation zone was compared to the energy required for breakage using the BWI equation that requires the work index for granite and the 80 percent passing size for feed (F, initial size, in μm) and product (P, final size, in μm).

The bond energy calculation is sensitive to how particle size is defined, especially in this case for the anisotropic particles in zone 1. If the particles are defined by the length, the product 80 percent passing size is 60 mm, and the Bond energy is found to be 899 J. These calculations of Bond energy are consistent with the energy of 848 J measured for fragmentation during high-velocity impact.

Table 1 — Particle size analysis of granite core fragmentation zone, with length as the characteristic dimension.

Particle length class (mm)	Weight (percent)	Cumulative percent passing
>100	3.91	100.00
100 × 70	8.31	96.09
70 × 50	14.65	87.78
50 × 35	6.16	73.12
35 × 25	8.11	66.96
<25	58.85	58.85

Conclusions

High-velocity impact tests performed on granite bars were used to study damage as a function of energy dissipation. The results are of interest to explain blasting and comminution phenomena encountered in the mineral industry. XCT examination of the damaged bar revealed that damage occurred in three distinct zones identified as the fragmentation, fracture and elastic zones. The size and shape of particles in the fragmentation zone were found to be anisotropic, with elongation in the direction of energy propagation as the distance from impact increased. When the particles are defined by length rather than by sieve size, the energy absorbed is in agreement with that calculated from the BWI equation to about 5 percent. While good agreement of experimental energy for fragmentation and calculated BWI energy was found for the granite core, such agreement was not found for materials with porous textures such as limestone and concrete core bars. Results suggest that the texture of the core material is an important factor in the energy analysis. ■

References

1. Maxson W, Cadena F, Bond F (1933) Grindability of various ores, AIME, Trans. 112:130.
2. Johnson JC (2010) The Hustrulid bar—a dynamic strength test and its application to the cautious blasting of rock. PhD Dissertation, The University of Utah, Salt Lake City, UT

Petromineralogical studies of late Paleocene–middle Eocene phosphate nodules in the Subathu Basin of Solan District, Himachal Pradesh

Mohd Shuaib*, K.F. Khan, Samsuddin Khan and Shamim A. Dar
Department of Geology, Aligarh Muslim University, Aligarh, Uttar Pradesh, India
*Corresponding author email: shuaibamu16@gmail.com

Full-text paper:
Mining, Metallurgy & Exploration, https://doi.org/10.1007/s42461-019-0082-6

Keywords: Mineralogy, SEM micrographs, Phosphatic nodule, Subathu Formation, Fluorapatite

To read the full text of this paper (free for SME members), see the beginning of this section for step-by-step instructions.

Special Extended Abstract

This investigation of the petromineralogical studies of the late Paleocene–middle Eocene phosphatic nodules in the Dati-Dib area of Solan District is an attempt to study and observe the mineralogical characters, distribution pattern, texture and optical behavior of phosphate-bearing minerals and associated gangue in order to interpret the mode of their formation and depositional environment of the basin. The findings obtained from thin-section, X-ray diffraction (XRD) and scanning electron microscopy with energy-dispersive X-ray spectroscopy (SEM with EDX) studies indicate that the minerals' different forms, textures and distributions in phosphatic nodules might be due to environmental vicissitudes in oxidizing to reducing conditions followed by replacement processes. Various separation methods and flowsheets are used to separate phosphate from gangue minerals in phosphate nodules. Based on the phosphate and gangue minerals present in the nodules, low-temperature roasting at 400 to 600 °C, combined with dry magnetic separation and high-intensity electrostatic separation, are used to separate phosphate from organic matter, sulfide minerals and quartz. The most important fertilizers produced are single and triple superphosphates (SSP, TSP) and ammonium phosphates (MAP, DAP).

Background

The Subathu Formation in Solan District of Himachal Pradesh, northwest Sub-Himalaya, is famous for various geological and palaeobiogeographical aspects. The Subathu Formation has phosphorites that are found to occur in the form of pellets, ovulates, bone and replacement fragments, and phosphatic nodules (Fig. 1). Due to the paucity and high requirement of phosphorite, Dati-Dib and its adjoining areas have attracted prospecting from time to time.

The Subathu Formation is bounded by thrust on both sides, which appear as narrow strips. This formation is underlain by Kasauli Formation on the western and southwestern sides, and on the other side, it is underlain by the Basantpur Formation, which is folded in a synclines structure (Fig. 2). The Subathu Formation consists of limestones, shales and green mudstones. The rocks are rich in fossils, indicating a shallow marine environment. The Kasauli Formation is mainly characterized by predominant variegated sandstone and clay, whereas the Basantpur Formation comprises hard and massive dolomitic limestone and shale.

Materials and methodology

Using a polarizing microscope, a thin-section study was

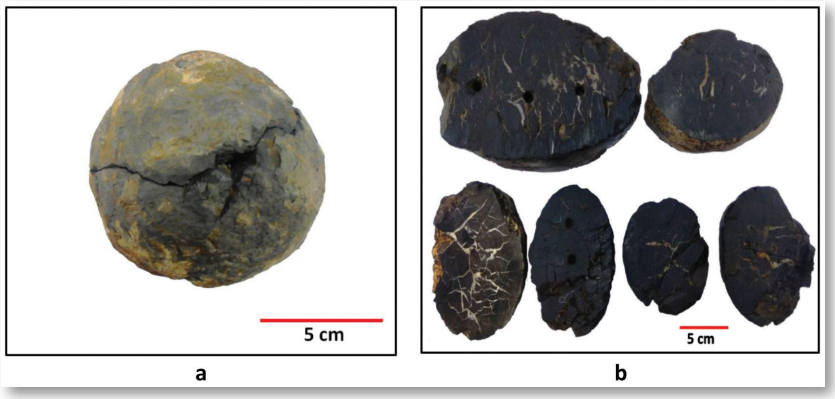

Fig. 1 Photographs of phosphate nodules from the Dati-Dib area of Solan District, Himachal Pradesh: (a) Hand specimen of phosphate nodules (b) Halves cut nodule sections.

performed to explore the optical behavior and mineralogical characters of the phosphorite nodules collected from the Dati-Dib area. The powdered nodule samples, of approximately 200 mesh size, were run through an XRD instrument to obtain diffractograms that were used to interpret mineralogy. The stub-fixed, freshly broken samples were coated with a thin coating of gold using a gold sputter coater. Prepared samples at diverse magnifications were examined under a JEOL JSM-6400 SEM attached with an energy-dispersive X-ray microanalyzer to interpret the crystal morphology, shape, size and nature of the mineral grains.

Results and discussion

Mineralogical studies of the phosphatic nodules reveal that phosphate minerals are found in the form of pellets or nodules and as a matrix of apatite in the groundmass composed essentially of the mineral fluorapatite ($Ca_5(PO_4)_3F$), which is the dominant phosphate mineral of phosphatic nodules typically found in cryptocrystalline nature in the Dati-Dib area. The phosphatic nodules contain organic matter, which imparts a brown to brownish-black color to the nodules. Dark-brown radiolaria, approximately 0.2 mm in size, are completely phosphatized. The test of the planktonic foraminifera is completely replaced by the silica material, and the internal part of the chamber is still preserved. Irregular grains or masses of pyrite are disseminated throughout the entire mass. Diffractometric analyses of selected phosphatic nodules reveal that the dominant minerals are fluorapatite and quartz with a minor amount of hydroxyl apatite. SEM observation of phosphatic nodules was performed on fractured

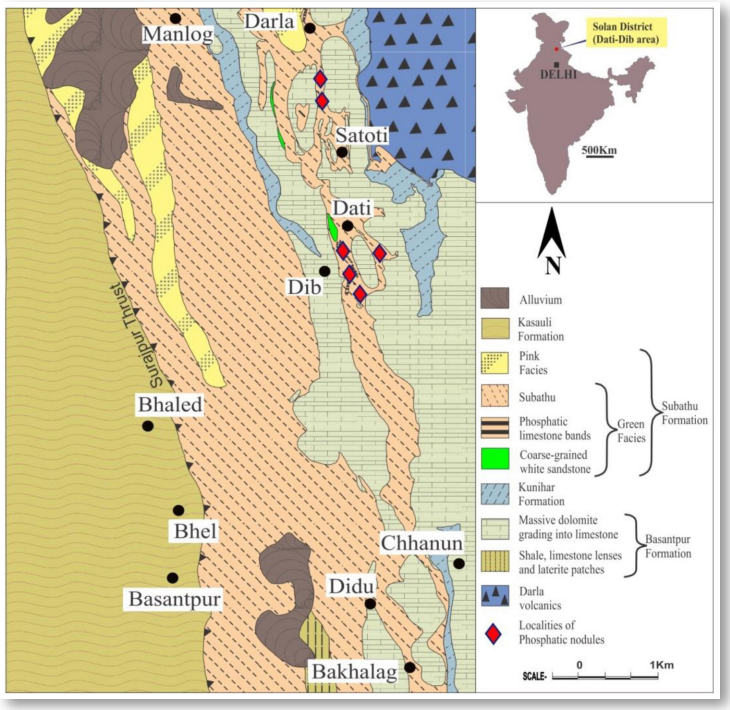

Fig. 2 Modified geological map of a part of Solan District, Himachal Pradesh (modified from [1]).

surfaces to observe the internal texture of the nodules. The presence of crystalline apatite in these nodules indicates that in initial stage, the phosphate was deposited as noncrystalline or least crystalline metastable phase, but later on, it was transformed into crystalline apatite, depending on the saturation of phosphate minerals. At places, independent rod-shaped detrital apatite grains, approximately 20 μm in size, are seen that might be a part of earlier formed phosphorites. Microbial filaments and phosphatized planktonic foraminifera are observed in the groundmass of cryptocrystalline apatite that indicate the initial stage of formation of phosphatic nodules in shallow marine environmental conditions. Later on, organic matter was decomposed, and dissolved sulfate reacted with detrital iron minerals, forming pyrite, which occurs as equigranular euhedral microcrystals. All of these findings indicate that the reducing depositional conditions were prevailing at the time of formation of these phosphatic nodules.

Conclusion

The phosphatic nodules of the Dati-Dib block of Solan District, Himachal Pradesh, are solely confined to the green facies of the Subathu Formation of Sirmur group. Thin-section, XRD and SEM with EDX studies reveal that fluorapatite is the dominant phosphate mineral of the apatite family. Silt-size silica is the predominant gangue mineral, whereas pyrite and muscovite are minor gangue minerals. The presence of organic matter gives a brown to brownish-black color to the phosphatic nodules. Phosphatized radiolaria and incomplete pyritized planktonic foraminifera were noted. The phosphate minerals appear as pellets, oolites and cryptocrystalline apatite in the groundmass. Original phosphatic matrix is replaced by the network of silica veins. Organic matter in the form of microbial filaments as revealed by SEM studies indicates the role of microorganisms in the formation of phosphatic nodules.

It is concluded from the thin-section, XRD and SEM with EDX studies that the mineral assemblages in the phosphatic nodules may have been initially formed in shallow marine environmental conditions, followed by reducing conditions with some environmental changes, replacement processes and biogenic activities. ■

References

1. Hasan SE, Srivastava RN (1968) Phosphorite investigation in Dati-Deeb area, Mahasu District, Himachal Pradesh. In: Geol Surv India, pp 1–42

Assessing the quality of incident investigations and its effect on safety performance: A study of the Ghanaian mining industry

Eric Stemn[1,2,*], Maureen E. Hassall[3], Carmel Bofinger[1] and David Cliff[1]

[1]Minerals Industry Safety and Health Centre, Sustainable Minerals Institute, The University of Queensland, Brisbane, Queensland, Australia

[2]Environmental and Safety Engineering Department, University of Mines and Technology, Tarkwa, Ghana

[3]The School of Chemical Engineering, The University of Queensland, Brisbane, Queensland, Australia

[*]Corresponding author email: e.stemn@uq.edu.au; estemn@umat.edu.gh

Full-text paper:
Mining, Metallurgy & Exploration, https://doi.org/10.1007/s42461-019-0076-4

Keywords: Investigation reports, Incidence rate, Causal factors, Corrective measures

To read the full text of this paper (free for SME members), see the beginning of this section for step-by-step instructions.

Special Extended Abstract

Incident investigation is of utmost importance in most high-risk industries and is often used to improve organizational safety. This study was undertaken to examine the content of past incident investigation reports to determine the effectiveness of the incident investigations. The study develops a semi-quantitative method to assess the effectiveness of incident investigations in the Ghanaian mining industry by evaluating the quality of past investigation reports. The assessment tool consists of five elements with several indicators and rating scales for assessing the quality of an investigation report as an indicator of the effectiveness of the investigation. The method was applied to 304 investigation reports of three Ghanaian large-scale gold mines, and the results correlated with incidence rates of the mines to determine if any relationship existed. The results showed that the mines differ significantly in the quality of their investigation reports, suggesting differences in the effectiveness of their investigations. In addition, the incidence rates of the mines negatively correlated with some elements of the assessment tool. In general, the method was found to be practically useful, as it is able to identify areas where incident investigation improvements are needed.

Background

The learning-from-incidents process models the plan-

act-check-do approach of management systems, often consisting of four major stages: (1) data collection and incident analysis, (2) planning interventions, (3) implementing interventions and follow-ups, and (4) evaluation. Incident investigations and analyses have been recognized as one of the vital stages of the learning process, because it is the stage where lessons are identified [1-3]. It has also been reported in the literature that results of the previous stage of the learning process are important for the next stage [1]. For instance, ineffective incident analyses could result in the planning of ineffective remedial measures, which subsequently may affect safety. One of the primary aims of incident investigations is to identify lessons from previous incidents which, when implemented, can prevent future recurrences or minimize the effects of future incidents. Organizations therefore need to assess the quality of their investigations periodically, as it is one of the notable means for improving workplace safety. Over the years, there has been a lack of focus on the effectiveness of incident investigations. This study was therefore initiated to contribute to this gap, focusing more closely on the quality of past incident investigation reports.

Method

An assessment tool was developed based on the works of Jacobsson, Ek and Akselsson [2] and Itoh, Omata and Andersen [4] and by adding elements specific to incident investigation reports collected from six large-scale Ghanaian gold mines. The assessment tool consists of: (1) elements, (2) indicators of each element and (3) a rating scale for assessing the effectiveness of each element based on the indicators.

The elements are various components of an investigation report, and five elements were defined after reading through 450 investigation reports. The elements, in turn, contain several indicators that should be covered in an investigation report. To be able to analyze an incident to determine what the causes were and recommend measures for preventing future events, a good description of the incident with relevant data is a prerequisite. Therefore, as a minimum, an investigation report should contain information on the incident itself, the circumstance surrounding the incident, the causes of the incidents and recommendation of measures for preventing future events. The first element — *general information* — focuses on the characteristics of victims, incident, equipment involved and those conducting the investigation. The second — *incident description* — consists of a detailed description of the incident and the circumstances surrounding it. The third — *time-band description* — focuses on details of the sequence of events leading up to and when the incident was resolved. The fourth and fifth elements, respectively, concern the *causal factors* and the *corrective measures* proposed following the identified causes. In order to assess and express the quality of an investigation report for the various elements numerically, a semi-quantitative rating scale of 1 to 10, divided into four quality levels, was developed. In using the scale, the assessor compares the information in the actual investigation report with the description in the scale, and the level best matching the actual description is selected. The assessment tool was then applied to 304 investigation reports of three large-scale Ghanaian gold mines to determine the quality of their investigations and the usability of the assessment tool.

Results

Figure 1 shows a distribution of the quality of investigation scores for each of the five elements of the assessment tool and the global score. The figure exemplifies characteristics from the lowest (1-2 Poor) to the highest (8-10 Excellent) quality level of the investigation reports. Across all the mines, the elements measuring the causal factor and corrective measures exhibited the most characteristics of the lower levels (Poor to Fair) and the least characteristics of the highest level (Excellent).

Discussions and conclusions

Across all the mines, the general information element scored highest, while causal factors and corrective measures

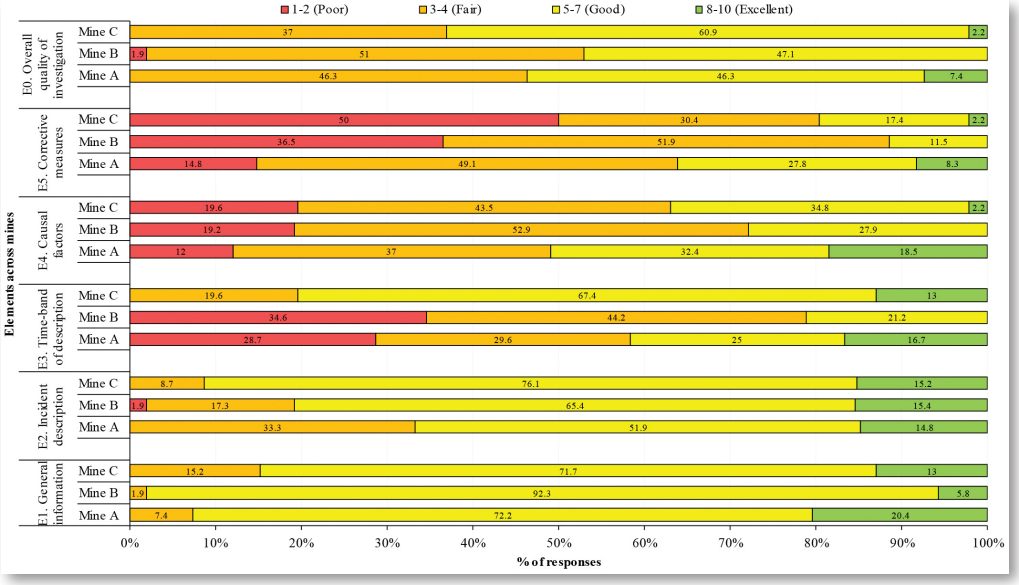

Fig. 1 Comparison of the quality of investigation levels across the three mines.

scored the lowest. This indicates that across the mines, there is a focus on describing an incident scenario and identifying those involved in an incident. However, when it comes to the most important stage of identifying the causes of an incident and proposing solutions, there is less focus. The identified causes often had a local view, focusing on the proximate causes in contrast to the distal causes. Again, the result further suggests that, even when distal causes are identified, the solutions proposed remain shallow, addressing mostly the immediate causes, leaving the distal causes unaddressed. Furthermore, the mines underutilize timeline when describing an incident. There was often no description of the events leading up to the incident, when the incident happened, and when the incident was resolved. The use of timelines to describe the incident events have been found to be a key feature of effective investigations [5]. This is because describing an incident with a timeline is an effective means of summarizing relevant information about the incident. Particularly, when the timeline description is represented graphically, it has been found to be useful in identifying data gaps, enabling an effective analysis of the incident during the search for causes. ■

References

1. Drupsteen L, Groeneweg J, Zwetsloot GIJM(2013) Critical steps in learning fromincidents: using learning potential in the process from reporting an incident to accident prevention. Int J Occup Saf Ergon 19(1):63–77. https://doi.org/10.1080/10803548.2013.11076966
2. Jacobsson A, Ek Å, Akselsson R (2012) Learning from incidents – a method for assessing the effectiveness of the learning cycle. J Loss Prev Process Ind 25(3):561–570. https://doi.org/10.1016/j.jlp.2011.12.013
3. Lindberg A-K, Hansson SO, Rollenhagen C (2010) Learning from accidents – whatmore dowe need to know? Saf Sci 48(6):714–721. https://doi.org/10.1016/j.ssci.2010.02.004
4. Itoh K, Omata N, Andersen HB (2009) A human error taxonomy for analysing healthcare incident reports: assessing reporting culture and its effects on safety performance. J Risk Res 12(3–4):485–511. https://doi.org/10.1080/13669870903047513
5. Katsakiori P, Sakellaropoulos G, Manatakis E (2009)Towards an evaluation of accident investigation methods in terms of their alignment with accident causation models. Saf Sci 47(7):1007–1015. https://doi.org/10.1016/j.ssci.2008.11.002

Towards a field-portable, real-time organic and elemental carbon monitor

D. A. Parks[1,*], K.V. Raj[1], C.A. Berry[1], A.T. Weakley[2], P.R. Griffiths[3] and A.L. Miller[1]

[1]CDC NIOSH, Spokane, WA, USA

[2]University of California Davis, Davis, CA, USA

[3]Griffiths Consulting LLC, Ogden, UT, USA

[*]Corresponding author email: dparks@cdc.gov

Full-text paper:
Mining, Metallurgy & Exploration (2019) 36:765–772, https://doi.org/10.1007/s42461-019-0064-8

Keywords: Diesel particulate matter, Organic carbon, Elemental carbon, Real-time monitor

To read the full text of this paper (free for SME members), see the beginning of this section for step-by-step instructions.

Special Extended Abstract

Diesel particulate matter (DPM) has been classified as a carcinogen to humans by the International Agency for Research on Cancer. DPM exposure is therefore regulated by the U.S. Mine Safety and Health Administration (MSHA). The current monitoring process takes days or weeks for exposure levels to be known, and a real-time monitoring device is needed. It is believed that infrared spectroscopy has potential for use in a real-time, field-portable device. This paper presents a method for measuring organic carbon (OC) and elemental carbon (EC) in DPM for a broad range of OC/EC ratios.

Introduction

A permissible exposure limit (PEL) for DPM of 160 µg/m^3, in terms of time-weighted average over eight hours, of total carbon (TC) was instituted for U.S. mines by MSHA in 2008. Although typical levels in mines have been decreasing since the implementation of the PEL, DPM overexposures continue to occur (Fig. 1).

Previous efforts have sought to develop a real-time DPM monitor [1-3], resulting in several commercially available instruments that measure light extinction in the optical regime which, under ideal circumstances, can be attributed to EC. To obtain TC from EC, one must assume that OC is proportional to EC with a known constant of proportionality. OC/EC ratios have been shown to be roughly constant for aerosols derived from different sources [4]. In principle, this implies that TC may be estimated, given knowledge of EC for a particular source, to the first approximation. However, it is important to pay close attention to OC/EC ratios as there is evidence they may deviate due to the use of diesel exhaust after-treatment technologies and the increasingly widespread use of biodiesel [5].

In this study, diffuse before transflection infrared spectroscopy is used to quantify OC and EC as defined by the

NIOSH 5040 method of the U.S. National Institute for Occupational Safety and Health (NIOSH). It should be noted that there have been other successful quantifications of carbonaceous aerosols by way of Fourier transform infrared (FT-IR) spectroscopy. However, the data presented here are unique in that they represent the first FT-IR prediction of OC and EC as defined by the NIOSH 5040 method. Further, in this study, collocated samples were not needed — rather, the same filter on which the 5040 analysis was performed was analyzed directly by way of FT-IR. In this way, artifacts such as the loss of semivolatile organic carbon are avoided.

Research method

DPM sampling. To simulate the evolving nature of DPM — specifically, the potentially more diverse array of OC/EC ratios [6] — several different sampling methods/sources were used in this study. Some of the data were generated using a laboratory-based system, specifically designed for collecting tailpipe samples from a variety of diesel engines. In addition to these laboratory-generated samples, 60 samples were obtained from within two different operating mines.

Infrared spectrometry. The mid-infrared spectrum of each DPM-loaded quartz fiber filter was measured immediately prior to the filter being placed into a Sunset Laboratory Inc. organic carbon/elemental carbon laboratory instrument model 5L for analysis. The spectra were measured using a Bruker Alpha FT-IR spectrometer equipped with a diffuse reflection accessory that incorporated a gold mirror backing.

Processing of infrared spectra for determining organic carbon. It was observed previously [7] that the aliphatic C-H stretching bands were a good candidate for quantification of organic carbon. In an effort to improve the model, a Monte Carlo algorithm was used (within the aliphatic region) to develop an improved linear regression model. The resulting model correlates quite well with the 5040 OC, having r^2 = 0.96 for the diverse range of OC/EC ratios for samples

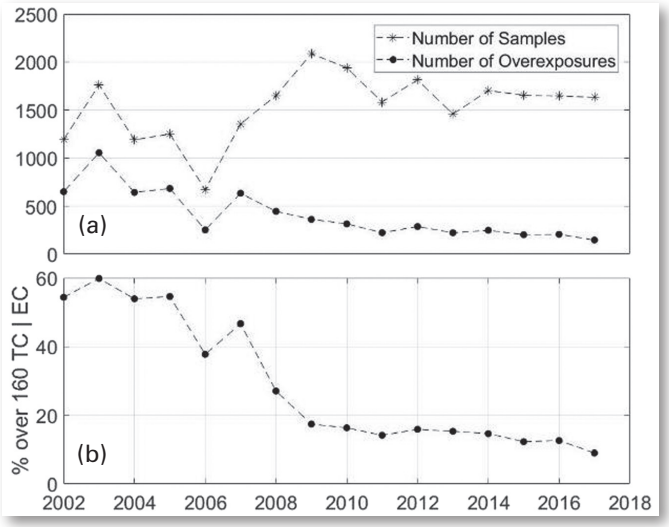

Fig. 1 (a) Number of DPM compliance samples taken by MSHA per year and (b) percentage of those samples with TC > 160 µg/m³.

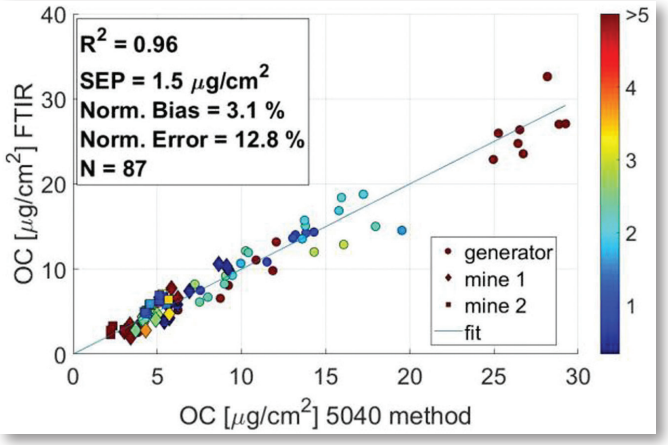

Fig. 2 Correlation between OC and the multiple regression peaks. The color bar represents the ratio of OC to EC.

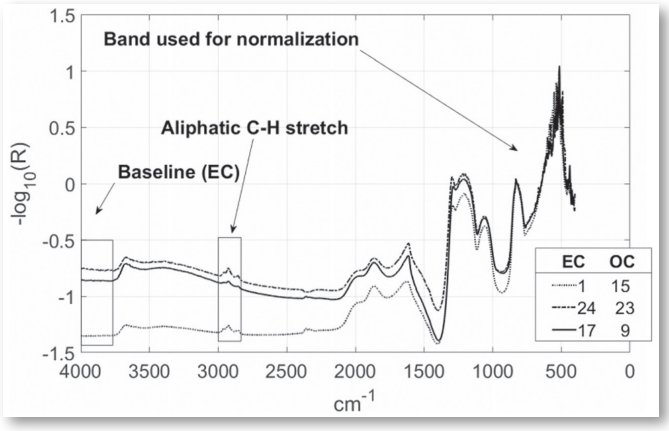

Fig. 3 Transflection spectra normalized to the 822 cm^{-1} peak. OC and EC are in µg/cm².

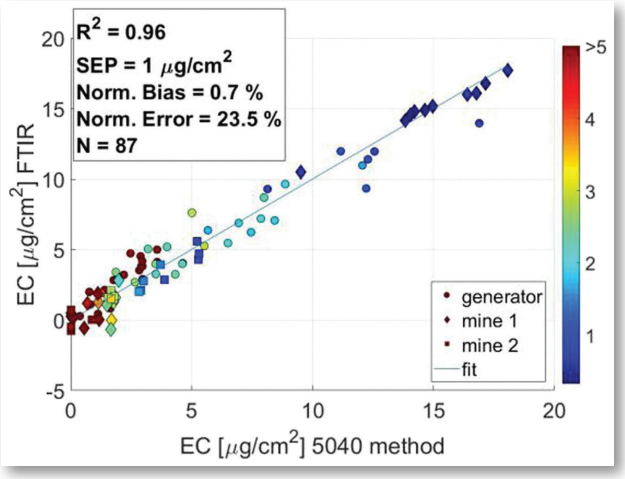

Fig. 4 Correlation between the height of the baseline, after normalization, and the 5040 EC values. The color bar represents the ratio of OC to EC.

collected in mines or in the laboratories ( ). Therefore, one calibration may be used to measure OC over a large range of OC/EC ratios. Note that the color bar in [illegible] represents the ratio of OC to EC.

Processing of infrared spectra for determining elemental carbon. When processing infrared spectra to determine EC, the particle size of DPM is typically so small (approximately 100 nm) and the layer of DPM so thin (less than 2 μm) that the deposited DPM contributes minimally to the scattering, most of which arises from the quartz fiber filter. Because the morphology of these filters varies slightly from sample to sample, their scattering coefficient, and hence the baseline of the transflectance spectrum, will also vary. Thus, the spectrum must be normalized prior to quantifying the OC and EC contents. In this study, the spectra of quartz fiber filters were normalized to the silica peak at 822 cm^{-1} as illustrated in Fig. 3.

When this normalization is performed, it is found that the broad electronic absorption band of deposited polycyclic aromatic hydrocarbons and graphitic material increases the value of the apparent baseline between 3,900 and 4,000 cm^{-1}, and that the average value of $-\log_{10} R(\tilde{\nu})$ in this region correlates with EC loading on the filter, as can be seen in Fig. 4.

Summary

This result opens the door to a potential FT-IR-based device that collects an air sample onto a filter medium and analyzes it for EC and OC in near-real time. In essence, the selection of a few bands also sets the stage for a multichannel device based on an infrared source and detector that target the bands of interest. ■

Disclaimer

The findings and conclusions in this report are those of the authors and do not necessarily represent the official position of the National Institute for Occupational Safety and Health, Centers for Disease Control and Prevention. Mention of any company or product does not constitute endorsement by NIOSH.

References

1. Noll J, Janisko S, Mischler SE (2013) Real-time diesel particulate monitor for underground mines. Analytical Methods 5(12):2954-296
2. Noll JD, Janisko S (2013) Evaluation of a Wearable Monitor for Measuring Real-Time Diesel Particulate Matter Concentrations in Several Underground Mines. Journal of Occupational and Environmental Hygiene 10(12):716–722
3. Hansen A, Rosen H, Novakov T (1984) The aethalometer—an instrument for the real-time measurement of optical absorption by aerosol particles. Science of the Total Environment 36:191–196
4. Khan B et al (2012) Differences in the OC/EC ratios that characterize ambient and source aerosols due to thermal-optical analysis. Aerosol Science and Technology 46(2):127–137
5. Harrison RM et al (2013) An evaluation of some issues regarding the use of aethalometers to measure woodsmoke concentrations. Atmospheric Environment 80:540–548
6. Burtscher H (2005) Physical characterization of particulate emissions from diesel engines: a review. Journal of Aerosol Science 36(7):896–932
7. Parks DA, Miller AL, Chambers AJ, and Griffiths PR (2018) Investigation of spectroscopic methods for monitoring diesel particulate matter. in SME Annual Conference & Expo Feb. 25–28. 2017. Minneapolis, MN

Isothermal reduction kinetics and mechanism of pre-oxidized ilmenite

Yingyi Zhang[1,2,*], Jie Zhao[1], Xiaolong Ma[3], Mingyang Li[1], Yan Lv[4], Xudong Gao[2]

[1]School of Metallurgical Engineering, Anhui University of Technology, Maanshan, Anhui Province, China
[2]College of Material Science and Engineering, Chongqing University, Chongqing, China
[3]College of Chemistry and Bioengineering, Guilin University of Technology, Guilin, Guangxi Province, China
[4]Metallurgical Technology Institute, Central Iron and Steel Research Institute, Beijing, China
[*]Corresponding author email: zhangyingyi@cqu.edu.cn

Full-text paper:
Mining, Metallurgy & Exploration (2019) 36:825–837, https://doi.org/10.1007/s42461-019-0075-5

Keywords: Kinetics, Pre-oxidized ilmenite, Isothermal reduction, Carbon monoxide, Thermogravimetric analysis

To read the full text of this paper (free for SME members), see the beginning of this section for step-by-step instructions.

Special Extended Abstract

This study aims to investigate the reduction thermodynamics of ilmenite and pre-oxidized ilmenite, and reveals the isothermal reduction kinetics of pre-oxidized ilmenite concentrate by carbon monoxide. The results indicate that the ilmenite concentrate and pre-oxidized ilmenite concentrate can be selectively reduced by controlling the temperature.

The pre-oxidation process leads to the breakage of complex mineral structure, and the formation of porous simple oxides, which is an effective method to increase the reduction and leaching rate.

Background

Ilmenite is the main source of material for the production of metallic titanium and titanium-containing compounds [1]. Panzhihua, located in Sichuan in southwest China, has one of the largest ilmenite resources in the world, with an estimated ilmenite reserve of about 870 million tons, accounting for more than 90 percent of the total reserve in China and more than 35 percent of the total reserve in the world [2-3]. As sources of high-grade titaniferous ores are decreasing in the world, the reduction and utilization of low-grade ilmenite (40–50 percent TiO_2) has attracted attention. This paper's aim is to evaluate the isothermal reduction kinetic models of pre-oxidized ilmenite, and to investigate the influence of reduction temperature on the reduction degree, kinetic model and apparent activation energies.

Materials and methodology

The ilmenite concentrate was provided by Panzhihua Iron & Steel Co. (Sichuan Province, China). The reduction experiments are carried out on a Setaram Evo TG-DTA 1750 thermal analyzer. The reduction of samples (pre-oxidized ilmenite concentrate) was performed in the furnace, and the weight losses were measured by a thermo-balance with a sensitivity of $\pm 10^{-4}$ g in order to determine the extent of the reactions. The samples were put in the Al_2O_3 crucible and the weight of each sample was 30 ± 0.5 mg. When the samples were heated to the required temperature at a heating rate of 25 K/min, the samples were reduced in a flowing carbon monoxide (CO, 6 mL/min) and nitrogen (N_2, 14 mL/min) atmosphere, and the isothermal reduction temperatures were 1,073, 1,123, 1,173 and 1,223 K, respectively.

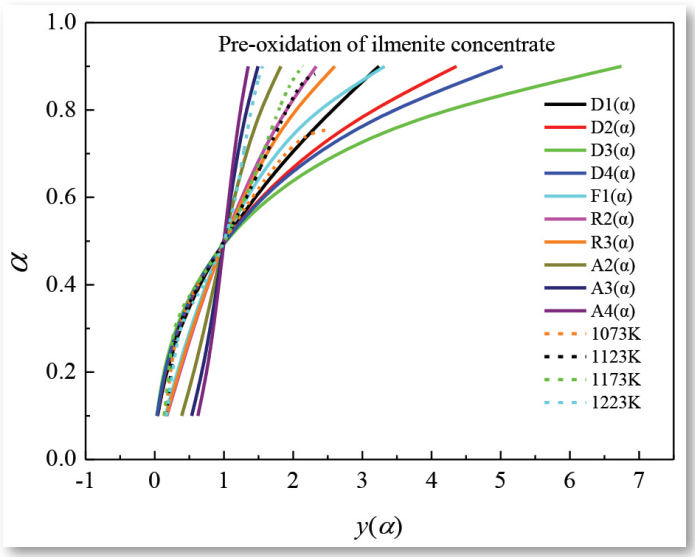

Fig. 1 Standard kinetics curves and fitting curves for samples at different temperatures.

Key results

Effect of pre-oxidized process on mineral composition. The pre-oxidation process leads to the breakage of the complex mineral structure of ilmenite concentrate, and the formation of porous simple oxides. The original ilmenite concentrate was oxidized into a mixture of rutile (TiO_2), pseudobrookite (Fe_2TiO_5) and magnesium titanate ($MgTi_2O_5$) with a steady flow of air for 2 h at 1,100 °C.

Effect of pre-oxidized process on isothermal reduction. The pre-oxidized ilmenite concentrate has higher reducibility than the original ilmenite in a carbon monoxide atmosphere. The reaction finishing time of pre-oxidized ilmenite concentrate was 50 percent less than that of the ilmenite concentrate.

Isothermal reduction process can be divided into three stages. In the first stage, the conversion degree increases sharply with increasing time. The reduction process is controlled by the random nucleation and subsequent growth model (A_2 model). In the second stage, the conversion degree increases slowly with increasing time. The reduction process is controlled by the diffusion of carbon monoxide in the reduced layer (D1 model). In the third stage, the conversion degree increases sharply with increasing temperature. The temperature has a greater effect on the reduction mechanism. The reduction processes at different temperatures are controlled by the diffusion of carbon monoxide in the reduced layer (1,073 K and D1 model), phase boundary chemical reaction (1,123 K and R_2 model), random nucleation and subsequent growth (1,173 to 1,223 K, A_2 and A_3 models), respectively. For the whole reduction process, the average apparent activation energies obtained by the isoconversional method and model-fitting method are 71.72 and 31.92 kJ·mol^{-1}, respectively. ■

References

1. Zhang WS, Zhu ZW, Cheng CY (2011) A literature review of titanium metallurgical processes. Hydrometallurgy 108: 177-188.
2. Liu YM, Qi T, Chu JL, Tong QJ, Zhang Y (2006) Decomposition of ilmenite by concentrated KOH solution under atmospheric pressure. Hydrometallurgy. 81: 79-84.
3. Chen DS, Song B, Wang LN, Qi T, Wang Y, Wang WJ (2011) Solid state reduction of Panzhihua titanomagnetite concentrates with pulverized coal. Miner Eng 24: 864-869.

Influence of air gap volume on achieving steady-state velocity of detonation

Eugie Kabwe[1,2,*]
[1]School of Civil, Environmental and Mining Engineering, The University of Adelaide, Adelaide, Australia
[2]Department of Mining Engineering, School of Mines, University of Zambia, Lusaka, Zambia
[*]Corresponding author emails: eugie.kabwe@adelaide.edu.au; kabweeugie@yahoo.com

Full-text paper:
Mining, Metallurgy & Exploration, https://doi.org/10.1007/s42461-019-0095-1

Keywords: Collar zone, Dáutriche technique, Explosive column, Top air-deck, Blasting, Confinement, Density, Emulsion, Velocity of Detonation

Special Extended Abstract

The velocity of detonation (VOD) is a significant property considered when rating an explosive, and it is quantified as a confined or unconfined velocity. The confined velocity is more significant as explosives are usually used under a definite degree of confinement. This study evaluates the stepwise increment of the air-deck volume from 10 to 30 percent, and its effect on the VOD. The VOD estimation in the 172-mm-diameter explosive column was conducted using the Dáutriche technique. The air-deck volume increment has an attenuation effect on the steady-state VOD, and detonation failure is high at 30 percent air-deck volume. This attenuation effect is directly linked to the explosive's rating and efficacy. The air-decking approach in this study is different from conventional air-decking techniques in that it does not employ the fixed blasthole parameters, air-deck volume and specific VOD.

Background

VOD is the rate at which detonation waves travel through an explosive column. For emulsion explosives, it varies between 4,000 and 5,500 m/s [1], depending on parameters such as blasthole diameter, confinement, particle size and explosive density. When an explosive detonates, a high-velocity shock wave and a tremendous release of gas that propagates within the native medium are induced. This process is a four-phase, rapid decomposition comprising initiation, deflagration, deflagration to detonation, and detonation [2]. The VOD values of a variety of commercial explosives are usually nonideal and are affected by factors such as the interface between fuel and oxidizer, charge diameter, degree of confinement and particle size [3-6]. This study evaluates the effects of increasing the air-deck volume on the VOD. The VOD is estimated in blastholes with different top air-deck volume using the simple Dáutriche technique. The top air-deck volume is increased stepwise by reducing the stemming height.

The VOD indicates the shock energy generated by the explosive that is used for rock fragmentation, also converted into seismic energy, acoustic energy and heat [7]. Berta [8] suggested that the transfer of this energy is a function of rock and explosive characteristics. Feng and Ze-gong [9] showed that when explosive blasting is conducted and the hole depth is below the critical depth, the blast energy accounts for 1/40th of the entire explosive energy. Only 23 to 37 percent of the rest of the blasting energy is used to expand the cavity of joints in a rock mass. The rest is transformed into other forms. The conventional practice of blasthole explosive is to charge to about two-thirds of the hole depth and stem the remaining one-third for explosive confinement (Fig. 1). Keeping the explosive level lower than two-thirds results in poor collar zone fragmentation [10-11].

Methodology

The blast trial was conducted using 18 blastholes charged with booster-sensitive bulk emulsion HEF100. Top column air-decks that served as stemming enhancers and prevented energy and gases from escaping from the blasthole were then introduced (Fig. 2). The energy that would otherwise have been lost was directed into the material being blasted and used more efficiently for stemming zone fragmentation.

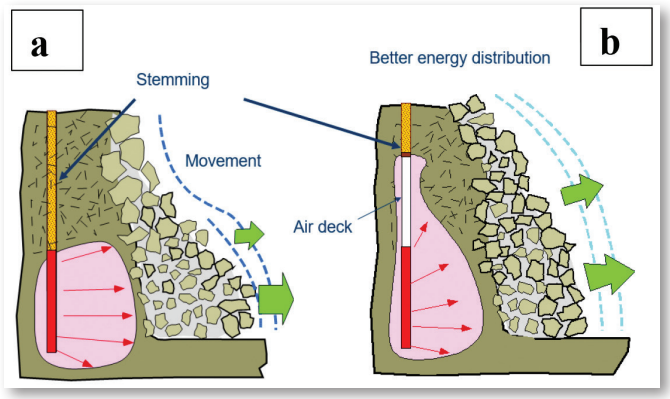

Fig. 1 Blast fragmentation using (a) conventional and (b) air-deck blast.

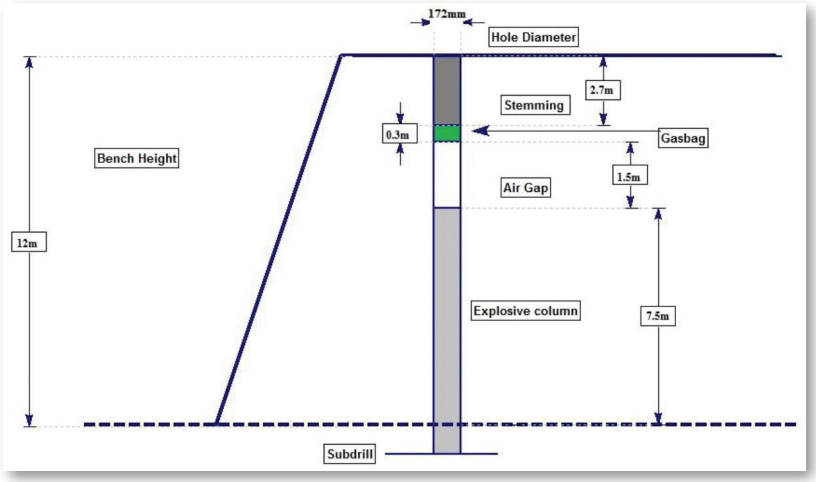

Fig. 2 Top air-deck column blast hole design.

The air-deck volume was increased by the reduction of the stemming volume while keeping the emulsion explosive volume and density constant. The air-deck occupied 1.5 m of the blasthole depth (12.5 percent of air-deck volume) as the standard procedure. In this study, the air-deck was initially set at a depth of 1.2 m (10 percent of volume), which was increased in steps to 3.6 m (30 percent).

Using the Dáutriche technique, the VOD estimation was attained with a detonating fuse bound onto an aluminium plate where detonation waves collide. A 0.005-m^2 aluminium plate was used to estimate the detonation waves by marking their impact. The difference between the mid-mark and impact mark obtained from the collided detonation waves was measured on the aluminium plate. The advantage of this technique is that it is suited to unconfined spaces where cartridge-form explosives are used [12].

Results and discussion

The trials were performed by replacing 10, 15, 20, 25 and 30 percent by volume of the blasthole with air-decks. The results are presented in Table 1 and Fig. 3.

The aim was to investigate the influence of the air-deck volume on the VOD in order to obtain optimum values for both the steady-state VOD and the air-deck volume while keeping the cost of the blasting consumables as low as possible. It was observed that the VOD measured at 3,450 m/s was optimum and corresponded to 20 percent air-deck volume (2.4 m depth). This further reduced the stemming volume to about 66 percent (1.8 m) which, in turn, reduced the blasting costs. Employing air-decks improves collar zone fragmentation, reduces overpressure and vibration levels, and lessens overall blasting costs. It also influences the VOD.

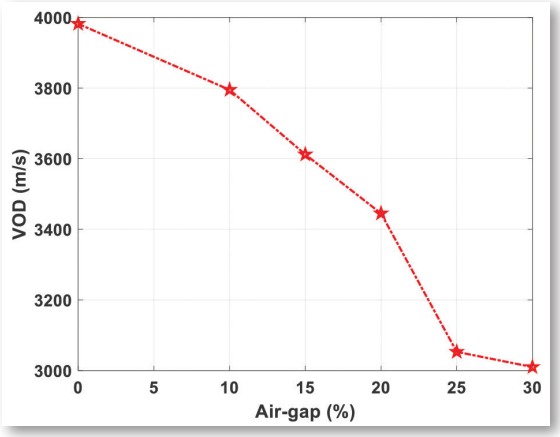

Fig. 3 Average steady-state VOD versus air-deck volume..

Conclusion

The study conducted based on a specific site, specific blasthole parameters and HEF100 emulsion explosives led to the following conclusions: (1) The VOD of the explosive column decreased with increasing percentage of the air-deck. The average VOD of the explosive at 20 percent air-deck replacement was about 3,450 m/s. (2) The reduction in the VOD was prominent after 20 percent air-deck volume, dropping to 3,053 m/s at 25 percent due to the cooling down of the reaction zone by the rarefaction from the air-decks. (3) The replacement with air-decks must be limited to 25 percent or less, depending upon the rock type, in order for this method of charging with air-decks to produce a stable detonation. ■

References

1. Pradhan GK, Pradhan M (2013) Explosive energy distribution in an explosive column through use of non-explosive material- case study. In Blasting in mines–new trends, the 10th international symposium on rock fragmentation by blasting, New Delhi. Taylor & Francis, pp. 81–89.
2. Bruckman HJ Jr, Guillet JE (1968) Theoretical calculations of hotspot initiation in explosives. Can J Chem 46(20):3221–3228.
3. Persson PA, Holmberg R, Lee J (1993) Rock blasting and explosives engineering. CRC Press, London.
4. Cunningham C (2005) Defining non-ideal performance for commercial explosives. Proc. 36th conference & exhibition, Institute of South Africa & ASPA, 3–5.
5. Crosby WA, Bauer AW, Warkentin JPF (1996) State of art explosive VOD measurement system, Proc. 7th annual conference on explosive and blasting, International Society of Explosive Engineers, pp. 23–34
6. Chiappetta RF (1998) Blast monitoring instrumentation and analysis techniques, with an emphasis on field applications. Fragblast 2(1):79-122
7. Spathis AT (2013) Innovations in blast measurement: reinventing the past. In rock fragmentation by blasting: the 10th international symposium onrock fragmentation by blasting, 2012. Fragblast 10 Taylor & Francis Books Ltd pp 23-39
8. Berta G (1990) Explosives: an engineering tool, Italesplosivi-Milano.
9. Feng C, Ze-gong L (2014) Energy distribution of columnar explosive blasting in rock. Electron J Geotech Eng 18:4221–4423
10. Kabwe E (2016) Improving collar zone fragmentation by top airdeck blasting technique. Geotech Geol Eng 35(1):157–167
11. Kabwe E (2018) Velocity of detonation measurement and fragmentation analysis to evaluate blasting efficacy. J Rock Mech Geotech Eng 10(3):523–533
12. Tete AD, Deshmukh AY, Yerpude RR (2013) Velocity of detonation (VOD) measurement techniques practical approach. International Journal of Engineering & Technology 2(3):259

Table 1 – Average VOD estimation with air-deck volume.

Air-deck (percent)	Average VOD (m/s)
10	3,795
15	3,612
20	3,445
25	3,053
30	3,010